

PAIR PLASMA PRODUCTION IN A FORCE-FREE MAGNETOSPHERE AROUND A SUPERMASSIVE BLACK HOLE

KOUCIHI HIROTANI¹ AND ISAO OKAMOTO²

Division of Theoretical Astrophysics, National Astronomy Observatory, Mitaka 181, Japan

Received 1997 January 1; accepted 1997 December 1

ABSTRACT

We quantitatively solve the problem of plasma supply to the stationary, axisymmetric, force-free magnetosphere of a rotating black hole residing in an active galactic nucleus. At the plasma source from which both inflowing and outflowing charge-separated plasmas originate, the shortage of charge will lead to the emergence of a strong electric field along the magnetic field line. The parallel electric field accelerates migratory electrons and/or positrons to ultrarelativistic energies. These relativistic electrons/positrons scatter background photons to produce high-energy γ -rays that can materialize as pairs by colliding with background photons. The produced pairs replenish the inflowing and outflowing charges and are accelerated to result in a stationary pair production cascade. It is demonstrated that a sufficient amount of plasma can be supplied for the Blandford-Znajek process to work effectively.

Subject headings: black hole physics — galaxies: active — galaxies: jets — plasmas

1. INTRODUCTION

The model of a stationary, plasma-filled magnetosphere around a rotating black hole and/or its accretion disk has been evoked to explain the extraction of energy in the vicinity of a black hole and the formation of relativistic jets observed in active galactic nuclei (Blandford 1976; Lovelace 1976; Blandford & Znajek 1977). For the recent observation of high-energy γ -ray emission from active galactic nuclei (AGNs), the Blandford-Znajek process is described as a viable mechanism for energizing the γ -ray jets (see, e.g., von Montigny et al. 1995 for a recent review of observations).

In the γ -ray-emitting region, relativistic jets must be dominated by the kinetic energy flux of e^\pm plasma over the electromagnetic flux originating from the central engine. A pair-cascade model of γ -ray jets has been proposed by Blandford (1993), Blandford & Levinson (1995, hereafter BL95), and Levinson (1996 and references therein). Their bulk jet dynamics for converting the Poynting flux to the kinetic energy is as follows: Once the bulk motion of the jets attains the Lorentz factor Γ larger than the threshold energy above which the opacity to pair production on the background photons exceeds unity, copious pair production would ensue, leading to a sharp increase in the inertia and radiative drag acting on the e^\pm outflow. This phenomenon is expected to occur above the annihilation radius r_{ann} for the e^\pm plasma (BL95).

On the other hand, in the region well below r_{ann} where rapid annihilation is dominating, the jet energy may well be regarded as predominantly electromagnetic. Levinson (1996) examined the structure of the “inner jet,” where the Poynting flux is being converted to the kinetic flux. By numerically solving the equation of motion for the bulk jet coupled with the appropriate kinetic equations governing the evolution of e^\pm pair and γ -ray number densities, he showed that for steep spectra, such as the standard spectrum invoked by BL95, the acceleration scenario predicts that the majority of the power extracted from the central engine will be emitted as soft X-rays rather than being converted into pairs and high-energy γ -rays, as required by the

observations. The spectrum incident on the inner jet must be sufficiently flat.

The source of the electromagnetic power eventually resulting in the γ -ray jet may be the spin of the central black hole (Blandford 1989, 1993). It is, however, the electric current that sustains the electromagnetic power in the field-dominated region of the magnetosphere, and it is charged particles, even though inertia-free, that carry the electric current. In other words, energy and angular momentum are transported out of the horizon by the electric current that can freely flow into and out of the horizon. However, even though under the assumption of masslessness, it must be real charged particles that constitute the electric current, and because no particle can classically escape beyond the horizon, electrons must flow into the horizon for the electric current to flow out, and positrons must flow into there for the electric current to flow in. We thus have to contrive a process of plasma supply deep within the magnetosphere that is somewhat different from the process of converting the Poynting flux into pairs and γ -rays in the jet much above the horizon.

We assume a stationary axisymmetric degenerate force-free magnetosphere around a rotating black hole. The absolute space around the hole with the mass M and the angular momentum J is described in a Boyer-Lindquist spatial coordinate system with the two scalar functions α and ω (Macdonald & Thorne 1982; Thorne, Price, & Macdonald 1986):

$$ds^2 = \frac{\rho^2}{\Delta} dr^2 + \rho^2 d\theta^2 + \varpi^2 d\phi^2,$$

where

$$\rho^2 = r^2 + a^2 \cos^2 \theta, \quad \Delta = r^2 - \frac{2GM}{c^2} r + a^2,$$

$$\Sigma^2 = (r^2 + a^2)^2 - a^2 \Delta \sin^2 \theta, \quad \varpi = \frac{\Sigma}{\rho} \sin \theta,$$

and

$$\alpha = \frac{\rho \Delta^{1/2}}{\Sigma}, \quad \omega = \frac{2aGM}{c \Sigma^2}; \quad (1)$$

¹ hirotani@ferio.mtk.nao.ac.jp.

² okamoto@nao.ac.jp.

a is the spin parameter defined by $a \equiv J/Mc$. The horizon radius is denoted by $r_H = GM/c^2 + [(GM/c^2)^2 - a^2]^{1/2}$. Here α is the lapse function or the redshift factor and ω is the angular velocity of so-called zero angular momentum observers (ZAMOs), which vanishes at infinity ($\alpha \rightarrow 1$) and coincides with the uniform rotation of the hole, $\omega_H \equiv c^3 a / (2GM r_H)$, at the horizon ($\alpha = 0$). The general relativistic effects on the force-free magnetosphere appear through α and ω .

Denoting the magnetic flux function as Ψ , one can define the poloidal magnetic field in terms of Ψ :

$$\mathbf{B}_p = -\frac{e_\phi \times \nabla \Psi}{2\pi\alpha}, \quad (2)$$

where e_ϕ is the unit toroidal vector. In the axisymmetric system the electric field is purely poloidal, and assuming the frozen-in condition, it is given by

$$\mathbf{E}_p = -\frac{\mathbf{v}_F \times \mathbf{B}_p}{c} = -\frac{\Omega_F - \omega}{2\pi\alpha c} \nabla \Psi, \quad (3)$$

where $\mathbf{v}_F = [(\Omega_F - \omega)\alpha/c]e_\phi$ is the rotational velocity of field lines measured by ZAMOs and $\Omega_F(\Psi)$ is the angular velocity of field lines.

The charge density in the degenerate force-free magnetosphere is given by the Goldreich-Julian charge density; i.e.,

$$\rho_{GJ} \equiv \frac{1}{4\pi} \nabla \cdot \mathbf{E}_p = -\frac{1}{4\pi} \nabla \cdot \left(\frac{\Omega_F - \omega}{2\pi\alpha c} \nabla \Psi \right) \quad (4)$$

everywhere except within the thin gap of the structure, which is our main concern. Since \mathbf{v}_F , and hence \mathbf{E}_p , changes sign at the surface where ω equals Ω_F , one can easily anticipate that ρ_{GJ} also changes sign in the vicinity of this surface. Some analyses reveal that ρ_{GJ} is negative far from the hole and positive near the hole along field lines near the rotation axis.

In a force-free magnetosphere, the “null surface” where ρ_{GJ} vanishes could be regions with a strong electric field (E_{\parallel}) sustained along a magnetic field line. If the charge density ρ_e differed significantly from ρ_{GJ} in any region, this would cause E_{\parallel} , which would act to move available charge into (from) the charge deficient (excess) region. However, near the null surface, there is not enough available charge to redistribute; this charge deficit leads to the emergence of E_{\parallel} .

A typical example of the distribution of the null surface is depicted in Figure 1. As the figure indicates, the null surfaces (solid lines) nearly coincide with the surface of $\omega = \Omega_F$ (dashed line). The magnetic field lines (dotted lines) are assumed to be radial in this figure, because the force-free transfield equation makes the field line structure be asymptotically radial for $\alpha \rightarrow 0$ (Macdonald & Thorne 1982; Okamoto 1992). For illustration purposes, Ψ is assumed to be proportional to $\sin^2 \theta$.

Under the existence of E_{\parallel} , The Poisson equation in the gap reads

$$\nabla \cdot \mathbf{E}_{\parallel} = 4\pi(\rho_e - \rho_{GJ}), \quad (5)$$

where $\rho_e \equiv e(n^+ - n^-)$ is the charge density viewed in the corotating frame of the magnetic field and is defined by the difference between positive and negative charges. Originally, Blandford & Znajek (1977) suggested the cascade mechanism for plasma supply. Migratory particles are accelerated by the near-vacuum electric field E_{\parallel} induced by

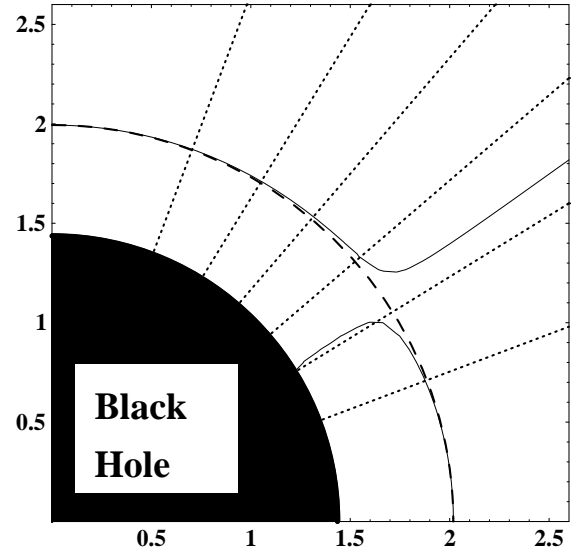


FIG. 1.—Distribution (side view) of the “null surface” where ρ_{GJ} vanishes around a rapidly rotating hole ($a = 0.9$ and $\Omega_F = 0.5\omega_H$). The magnetic field lines (dotted lines) are assumed to be radial near the horizon. In this figure, we adopt $\Psi \propto \sin^2 \theta$. The null surface (solid line) almost coincides with the surface of $\omega = \Omega_F$ (dashed line), except in the middle latitudes.

the rotation of the black hole, to relativistic energies, and these accelerated particles then inverse Compton scatter background photons from, e.g., the surrounding accretion disk. The resulting hard γ -ray photons collide with another background photons, to produce pairs of electrons and positrons, which fill the magnetosphere.

In spite of the core significance in feeding a relativistic γ -ray jet from the central engine, the real process of supplying charged particles in the magnetosphere has not been substantiated for a realistic model of radiation field in AGNs until Beskin, Istomin, & Par’ev (1992). For the typical parameters of the central radiation in AGNs, they estimated the width of the region of plasma production and the particle energies in it.

The purpose of this paper is to further extend the analysis of Beskin et al. (1992) and to clarify more quantitatively the micro process of interaction of radiation-pair creation under the existence of parallel electric field.

In the next section, we formulate basic equations describing a pair production cascade in the magnetosphere. We then solve them in § 3 and demonstrate that a sufficient amount of plasma is supplied by the cascade so that hole’s rotational energy may be extracted effectively. In the final section, we sum up the results and discuss the differences from Beskin et al.’s.

2. PAIR PRODUCTION CASCADE MECHANISM

In this section, we describe how a pair production cascade proceeds in a thin gap in the force-free magnetosphere. We first discuss physical processes in the potential gap leading to the cascade in § 2.1. We next formulate basic equations in § 2.2, discuss nongray analysis of the γ -ray distribution in § 2.3, and introduce boundary conditions in § 2.4.

2.1. Physical Processes

As we have discussed in the previous section, E_{\parallel} , the longitudinal electric field, can no longer be screened near

the null surface from which both the inflowing and outflowing charge separated plasmas originate, and a thin electrostatic potential gap will be formed there. Although B_p may, in general, be oblique to the gap surface, we consider the perpendicular case in which the acceleration of e^\pm s by E_\parallel , and hence the pair production cascade, will work most effectively. We can then rewrite the Poisson equation (5) into the form

$$\frac{dE_\parallel}{dx} = 4\pi[e(n^+ - n^-) - \rho_{GJ}], \quad (6)$$

where x is the outwardly increasing coordinate perpendicular to the null surface. For a spherical shape of the null surface, for instance, x is related with r as $x = (r - r_0)$, where r_0 is the radius at which ρ_{GJ} exactly vanishes. Moreover, as we shall see in § 3.1, the width of the potential gap in which E_\parallel is significant may be regarded as very thin compared with the hole's radius, $r_H \sim 10^{13.5}(M/10^8 M_\odot)$ cm. Therefore, we can expand $\rho_{GJ}(x)$ around $x = 0$ and obtain

$$\frac{dE_\parallel}{dx} = 4\pi[e(n^+ - n^-) - Ax], \quad (7)$$

where A is the expansion coefficient of ρ_{GJ} at $x = 0$ and on the order of $\Omega_F B/(2\pi ce)$. For a spherical null surface, again, we have $A = \partial_r(\rho_{GJ})$ at $x = 0$.

In the potential gap, the e^\pm s will rapidly lose their perpendicular momentum owing to Compton scatterings with ambient UV photons. (Unlike in a neutron star magnetosphere, synchrotron loss is negligible in a black hole magnetosphere because of its weak magnetic field.) However, their longitudinal motion will be maintained by the electrostatic acceleration due to E_\parallel field. Therefore, the motion of a single e^+ or e^- can be approximated one-dimensionally and obeys

$$m_e c^2 \frac{d\Gamma}{dx} = eE_\parallel - (\Gamma^2 - 1)\sigma_T U_b, \quad (8)$$

where Γ is the Lorentz factor of longitudinal motion, σ_T is the Thomson cross section, and U_b is the energy density of the background radiation field. The second term, which represents the Compton drag, may be overestimated to some degree; however, this simple expression has an advantage for our investigation of pair production mechanisms. Except for the vicinity of the boundaries of the gap at which E_\parallel vanishes, the right-hand side of equation (8) cancels itself in the leading order. Therefore, the longitudinal Lorentz factor attains its terminal value:

$$\begin{aligned} \Gamma(x) &= \sqrt{1 + \frac{eE_\parallel(x)}{\sigma_T U_b}} \\ &= 5 \times 10^3 \left[\frac{E_\parallel(x)}{10^3 \text{ V m}^{-1}} \right]^{1/2} \left(\frac{U_b}{10^6 \text{ ergs cm}^{-3}} \right)^{-1/2}. \end{aligned} \quad (9)$$

Note that we consider the case of $E_\parallel > 0$ in this paper. Newly created e^\pm s may have perpendicular momenta; however, they lose such momenta by scattering background radiation photons in a length

$$\begin{aligned} l_{\text{drag}} &= \frac{\Gamma m_e c^2}{\Gamma^2 \sigma_T U_b} = \frac{m_e c^2}{\sqrt{eE_\parallel(x)} \sigma_T U_b} = 2.5 \times 10^8 \\ &\times \left(\frac{E_\parallel(x)}{10^3 \text{ V m}^{-1}} \frac{U_b}{10^6 \text{ ergs cm}^{-3}} \right)^{-1/2} \text{ cm}. \end{aligned} \quad (10)$$

This length is smaller than the Compton mean free path at which e^\pm s scatter a background X-ray photon to produce a γ -ray photon that can lead to a pair production, $l_c \sim 10^{10}$ cm. We will confirm in § 3.1 that l_c is shorter than the gap half-width, H . It is possible to introduce two approximations from the fact $l_{\text{drag}} < l_c < H$: The e^\pm s migrate one-dimensionally and their motion is *monoenergetic* with a single Lorentz factor $\Gamma(x)$. The reason why $l_{\text{drag}} < l_c$ holds is that not only X-ray photons but also UV photons contribute to the drag. Therefore, for a very hard spectrum ($\alpha < 1$), l_{drag} roughly equals l_c , and the two assumptions presented above break down. The e^\pm s moving with a Lorentz factor such as given by equation (9) can emit high-energy γ -ray photons neither by curvature radiation nor by synchrotron radiation. Nevertheless, these e^\pm s can produce sufficient amount of high-energy γ -ray photons via *inverse Compton scatterings* of background X-ray photons (Beskin et al. 1992). In fact, from the energy conservation, the e^\pm s can produce γ -ray photons with energies up to

$$\Gamma m_e c^2 = 50 \left(\frac{\Gamma}{10^2} \right) \text{ MeV}.$$

Next, we focus attention on whether such γ -ray photons collide with background X-ray photons to produce pairs. In order that a γ -ray photon may produce an e^\pm pair by colliding with a background X-ray photon with energy $m_e c^2 \epsilon_s$, the γ -ray energy $m_e c^2 \epsilon_\gamma$ must satisfy

$$\epsilon_\gamma \epsilon_s \geq \frac{2}{1 - \mu}, \quad (11)$$

where μ is the cosine of the colliding angle between the γ -ray and the soft X-ray. The minimum γ -ray energy that can lead to a pair production is obtained by considering a head-on collision ($\mu = -1$) with the most energetic soft photon ($\epsilon_s = \epsilon_{\text{max}}$). That is, only γ -rays with energies above $\epsilon_\gamma^{\text{min}} \equiv 1/\epsilon_{\text{max}}$ can contribute to a pair production. If we take, for example, $\epsilon_{\text{max}} = 30 \text{ keV}/(mc^2) = 5.87 \times 10^{-2}$, we obtain $m_e c^2 \epsilon_\gamma^{\text{min}} = 8.7 \text{ MeV}$, which is much less than the maximum γ -ray energy produced by the inverse Compton scatterings, $\Gamma m_e c^2 \sim 50 \text{ MeV}$. Therefore, it seems reasonable to suppose that the γ -ray photons can produce the e^\pm pairs that lead to a pair production cascade in the potential gap.

So far, we have seen that relativistic e^\pm s accelerated in the potential gap upscatter background X-ray photons into γ -ray regimes and that such γ -ray photons collide with background X-ray photons to produce pairs, which may lead to a cascade. It is, moreover, entirely fair to say that e^\pm s and γ -ray photons move one-dimensionally along the magnetic field and that the e^\pm spectrum is monoenergetic at a certain position. Under these conditions, we formulate basic equations describing the pair production cascade in the next subsection.

2.2. Basic Equations

Let us first consider the continuity equations of e^\pm s. For simplicity, we shall suppose that positrons are migrating outward while electrons are migrating inward. Such a situation will be realized in the low latitudes in Figure 1. In the high latitudes, on the other hand, e^\pm s migrate in the opposite direction. However, the same formulation as presented below can also be applied, if one notices that not only the sign of $(n^+ - n^-)$ but also those of both dE_\parallel/dx and ρ_{GJ} in equation (6) change in the high latitudes. That is, the treatment made in this paper is valid irrespective of

whether E_{\parallel} orients outward or inward. We consider the former case alone.

Under the assumption described above, all positrons (or electrons) migrate outward (or inward) with speed $c[1 - 1/\Gamma^2(x)]^{1/2}$ because we are considering monoenergetic spectrum of e^{\pm} s. Thus, the continuity equations become

$$\pm \frac{d}{dx} \left[n^{\pm}(x) \sqrt{1 - \frac{1}{\Gamma^2(x)}} \right] = \int_0^{\infty} \eta_p(\epsilon_{\gamma}) [F^+(x, \epsilon_{\gamma}) + F^-(x, \epsilon_{\gamma})] d\epsilon_{\gamma}, \quad (12)$$

where the angle-averaged pair production redistribution function η_p is defined by

$$\eta_p(\epsilon_{\gamma}) \equiv \frac{1}{2} \int_{-1}^1 d\mu \int_{2/[(1-\mu)\epsilon_{\gamma}]}^{\epsilon_{\max}} d\epsilon_s \frac{dN_s}{d\epsilon_s} \sigma_p, \quad (13)$$

$$\sigma_p \equiv \frac{3}{16} \sigma_T (1 - v^2) \left[(3 - v^4) \ln \frac{1+v}{1-v} - 2v(2 - v^2) \right], \quad (14)$$

$$v(\mu, \epsilon_{\gamma}, \epsilon_s) \equiv \sqrt{1 - \frac{2}{1 - \mu \epsilon_{\gamma} \epsilon_s}} \quad (15)$$

(see Berestetskii, Lifshitz, & Pitaevskii 1989). Here σ_p refers to the cross section for pair production in a collision between photons with energies $m_e c^2 \epsilon_s$ and $m_e c^2 \epsilon_{\gamma}$, and moving at an angle $\cos^{-1} \mu$ to each other. $n^+(x)$ indicates the number density of outwardly moving particles, that is, positrons in this case, while $n^-(x)$ indicates that of inwardly moving particles, that is, electrons. $F^{\pm}(x, \epsilon_s)$ are the number density of γ -ray photons propagating in the $\pm x$ -directions, respectively, at a position x and in the nondimensional energy interval $\epsilon_{\gamma} \sim \epsilon_{\gamma} + d\epsilon_{\gamma}$; $dN_s/d\epsilon_s$ refers to the number density of background soft photons in the nondimensional energy interval $\epsilon_s \sim \epsilon_s + d\epsilon_s$. Only when two colliding photons satisfy condition (11) does σ_p has a nonvanishing value. It must be noted that the γ -ray photons, which are produced by the inverse Compton scatterings, are highly beamed in the same direction of e^{\pm} 's one-dimensional motion. That is, their distribution functions can be fully described in terms of F^+ and F^- .

We can easily see that the current, which is carried by e^{\pm} s along a given field line, is conserved along x . From one combination of equation (12), we have

$$\frac{d}{dx} \left\{ [n^+(x) + n^-(x)] \sqrt{1 - \frac{1}{\Gamma^2(x)}} \right\} = 0,$$

which yields

$$[n^+(x) + n^-(x)] \sqrt{1 - \frac{1}{\Gamma^2(x)}} = \frac{j_0}{e}, \quad (16)$$

where the current density j_0 is constant along a field line. In order that the energy and angular momentum may be extracted effectively from a rotating supermassive black hole, j_0 must take the value of

$$j_0 \sim 10^{-13} \left(\frac{a}{M} \right) \left(\frac{M}{10^8 M_{\odot}} \right) \left(\frac{B}{10^4 \text{ G}} \right) \text{ abamp cm}^{-2}. \quad (17)$$

in order of magnitude (e.g., Thorne et al. 1986). (If we multiply $c = 3 \times 10^{10} \text{ cm s}^{-1}$ to this value, we obtain a current density in the unit of statamp cm^{-2} .) The other com-

bination of equation (12) gives

$$\frac{d}{dx} \left\{ [n^+(x) - n^-(x)] \sqrt{1 - \frac{1}{\Gamma^2(x)}} \right\} = 2 \int_0^{\infty} \eta_p(\epsilon_{\gamma}) [F^+(x, \epsilon_{\gamma}) - F^-(x, \epsilon_{\gamma})] d\epsilon_{\gamma}. \quad (18)$$

Instead of equation (12), we use equations (16) and (18) in what follows.

We next derive the Boltzmann equations for the γ -ray photons. As we noted in the previous subsection, we may regard the γ -ray photons as directed only in the $\pm x$ -direction. Thus, the γ -ray distribution functions F^{\pm} obey

$$\pm \frac{\partial}{\partial x} F^{\pm}(x, \epsilon_{\gamma}) = \eta_c n^{\pm} \sqrt{1 - \frac{1}{\Gamma^2}} - \eta_p F^{\pm}, \quad (19)$$

where $\eta_c(\epsilon_{\gamma}, \Gamma)$ is the Compton redistribution function defined by

$$\eta_c \equiv \int_{\epsilon_{\min}}^{\epsilon_{\max}} d\epsilon_s \frac{dN_s}{d\epsilon_s} \sigma_{\text{KN}}(\epsilon_s, \Gamma) \delta(\epsilon_{\gamma} - \Gamma^2 \epsilon_s); \quad (20)$$

the Klein-Nishina cross section σ_{KN} is defined by (e.g., Rybicki & Lightman 1979)

$$\sigma_{\text{KN}}(z) \equiv \frac{3}{4} \sigma_T \left\{ \frac{1+z}{z^3} \left[\frac{2z(1+z)}{1+2z} - \ln(1+2z) \right] + \frac{\ln(1+2z)}{2z} - \frac{1+3z}{(1+2z)^2} \right\}, \quad (21)$$

Here, we implicitly assumed that the energy transfer from a positron or an electron with a Lorentz factor Γ to a photon with incident energy $m_e c^2 \epsilon_s$ is roughly $m_e c^2 \Gamma^2 \epsilon_s$ in equation (20); this treatment will be justified in order of magnitude. Of course, we could in general take its dependence on incident and scattered angles of photons into account and use a more precise Compton scattering kernel. However, to follow up such a detailed, complex argument further would take us beyond the scope of this paper. So, we adopt equation (20) as a Compton redistribution function.

The migrating e^{\pm} s and the γ -ray photons in the gap are described by differential equations (7), (8), (18), and (19). It is worth noting that n^+ and n^- are related by equation (16) and that equation (19) contains two independent equations. To integrate these five differential equations, however, we need to make some assumptions about the background radiation field.

We shall suppose that the spectral number density of background radiation per unit interval of ϵ_s can be represented by a single power law; i.e.,

$$\frac{dN_s}{d\epsilon_s} = C(\alpha) \epsilon_s^{-\alpha}, \quad (22)$$

where $C(\alpha)$ is a decreasing function of α and is defined by

$$C(\alpha) \equiv \frac{2 - \alpha}{\epsilon_{\max}^{2-\alpha} - \epsilon_{\min}^{2-\alpha}} \frac{U_b}{m_e c^2}; \quad (23)$$

ϵ_{\max} and ϵ_{\min} are the cutoff energies of the above spectrum. In what follows, we shall adopt

$$\epsilon_{\max} = \frac{30 \text{ keV}}{m_e c^2} = 5.87 \times 10^{-2}, \quad (24)$$

$$\epsilon_{\min} = \frac{10 \text{ eV}}{m_e c^2} = 1.95 \times 10^{-5}. \quad (25)$$

The energy density of the background radiation field, U_b , can be estimated as

$$U_b \sim \frac{L_b/c}{4\pi(5r_H)^2} = 1.47 \times 10^6 \left(\frac{M}{10^8 M_\odot} \right)^{-1} \left(\frac{L_b}{L_{\text{Edd}}} \right) \text{ ergs cm}^{-3}, \quad (26)$$

where L_b/L_{Edd} is the luminosity of the background radiation field normalized by the Eddington luminosity $L_{\text{Edd}} = 1.25 \times 10^{46} (M/10^8 M_\odot) \text{ ergs s}^{-1}$.

2.3. Nongray Analysis of γ -Ray Distribution

Since the redistribution function η_p varies with ϵ_γ , we cannot adopt a gray approximation for γ -ray distribution to solve the Boltzmann equations. Therefore, we will divide the γ -ray energy range into many bins and approximate η_p with its typical value in each bin.

Let β_i and β_{i-1} be the upper and lower limit of the i th nondimensional energy bin. Then taking β_i to be sufficiently close to β_{i-1} , one can approximate integrals in the right-hand side of equation (18) with the summation of the following integrals over each bin:

$$\int_{\beta_{i-1}}^{\beta_i} \eta_p(\epsilon_\gamma) F^\pm(x, \epsilon_\gamma) d\epsilon_\gamma \approx \eta_{p,i} f_i^\pm(x), \quad (27)$$

where

$$\eta_{p,i} \equiv \eta_p \left(\frac{\beta_{i-1} + \beta_i}{2} \right), \quad (28)$$

$$f_i^\pm(x) \equiv \int_{\beta_{i-1}}^{\beta_i} F^\pm(x, \epsilon_\gamma) d\epsilon_\gamma. \quad (29)$$

Then, instead of equation (18), we use

$$\frac{d}{dx} \left\{ [n^+(x) - n^-(x)] \sqrt{1 - \frac{1}{\Gamma^2(x)}} \right\} = 2 \sum_{i=1}^m \eta_{p,i} [f_i^+(x) + f_i^-(x)], \quad (30)$$

where m refers to the number of energy bins. Likewise, integrating equation (19) on ϵ_γ from β_{i-1} to $\beta_i (> \beta_{i-1})$, we obtain

$$\pm \frac{d}{dx} f_i^\pm(x) = \eta_{c,i}(\Gamma) n^\pm(x) \sqrt{1 - \frac{1}{\Gamma^2(x)}} - \eta_{p,i} f_i^\pm(x), \quad (i = 1, 2, \dots, m), \quad (31)$$

where

$$\eta_{c,i}(\Gamma) \equiv \int_{\beta_{i-1}}^{\beta_i} \eta_c(\epsilon_\gamma, \Gamma) d\epsilon_\gamma. \quad (32)$$

Consequently, we have a set of differential equations consisting of equations (7), (8), (30), and (31).

2.4. Boundary Conditions

The purpose of this paper is to elucidate the physical processes of the pair production cascade. To achieve this end, as a first step, we consider in this paper the case in

which the functions E_{\parallel} , Γ , n^+ , and f_i^\pm have such symmetric properties as described below.

First, $E_{\parallel}(x)$ should not change its sign in the gap and vanish at the two boundaries. Therefore, taking into account the fact that the width of the gap is very thin compared with r_H , we assume that E_{\parallel} is an even function of x ; i.e.,

$$E_{\parallel}(x) = E_{\parallel}(-x). \quad (33)$$

We also assume that $\Gamma(x)$ has the same symmetry:

$$\Gamma(x) = \Gamma(-x). \quad (34)$$

Second, from the assumption of symmetry, we impose

$$n^+(x) = n^-(-x). \quad (35)$$

The same may be true of γ -ray photons; we thus assume

$$F^+(x, \epsilon_\gamma) = F^-(-x, \epsilon_\gamma). \quad (36)$$

The solutions obtained under these symmetry properties will not miss the essential features of the pair production cascade in the black hole magnetosphere. In view of these symmetry properties, it follows that it is sufficient to solve equations (7), (8), (30), and (31) only in the range $0 \leq x \leq H$.

Let us now return to the derivation of boundary conditions at $x = 0$ and $x = H$. In the first place, from equations (8), (33), and (34), we have $d\Gamma/dx = 0$ at $x = 0$, which is equivalent to

$$E_{\parallel} = \frac{\sigma_T U_b}{e} \Gamma^2 \quad \text{at } x = 0. \quad (37)$$

In the second place, equations (35) and (16) give

$$2n^+ \sqrt{1 - \frac{1}{\Gamma^2}} = \frac{j_0}{e} \quad \text{at } x = 0. \quad (38)$$

Furthermore, we replace condition (36) for each ϵ_γ with

$$f_i^+ = f_i^- \quad (i = 1, 2, \dots, m) \quad \text{at } x = 0, \quad (39)$$

where f_i^\pm are defined by equation (29).

Let us next consider the conditions at the outer boundary of the gap. First, the *free* boundary, $x = H$, is defined so that E_{\parallel} vanishes there. That is,

$$E_{\parallel} = 0 \quad \text{at } x = H. \quad (40)$$

Second, any inwardly propagating particle (i.e., electrons in this case) should not come into the gap from the outside ($x > H$). This requires $n^-(H) = 0$, which combines with equation (16) to yield

$$n^+ \sqrt{1 - \frac{1}{\Gamma^2}} = \frac{j_0}{e} \quad \text{at } x = H. \quad (41)$$

Third, the charge density distribution must be continuous at $x = H$. We therefore impose from equations (41) and (7)

$$\frac{1}{4\pi} \frac{dE_{\parallel}}{dx} = j_0 \sqrt{1 - \frac{1}{\Gamma^2}} - Ax = 0 \quad \text{at } x = H. \quad (42)$$

Finally, no γ -ray photons come into the gap from the outside; therefore we readily find

$$f_i^- = 0 \quad (i = 1, 2, \dots, m) \quad \text{at } x = H. \quad (43)$$

We thus obtain total $(2m + 5)$ boundary conditions (37)–(43) for the $(2m + 3)$ unknown functions $E_{\parallel}(x)$, $\Gamma(x)$,

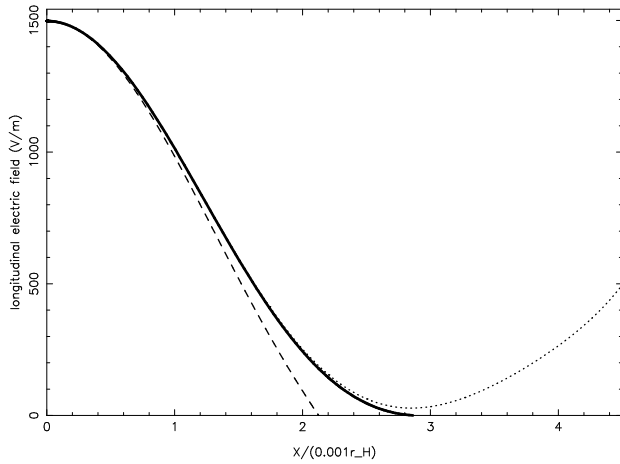


FIG. 2.—Variation of E_{\parallel} as a function of the position x along the field line when $U_b = 10^6$ ergs cm^{-3} and $\alpha = 2.0$. The abscissa is normalized by $10^{-3}r_H$, where $r_H = 10^{13.5}(M/10^8 M_{\odot})$ cm is the horizon radius. The solid line represents the solution of which derivative vanishes at $x = H$ with the “critical” current density $j_0 = j_{\text{cr}}$. The dashed line corresponds to $j_0 = 0.992j_{\text{cr}}$ and the dotted line to $j_0 = 1.0004j_{\text{cr}}$.

$n^+(x)$, and $f_i^{\pm}(x)$ ($i = 1, 2, \dots, m$) and two additional unknown constants H and j_0 . The reason why we regard j_0 as a unknown constant to be solved rather than an external, free parameter will be explained in detail later in this subsection.

To investigate the pair production mechanism, it is sufficient to consider γ -ray photons with nondimensional energies satisfying

$$\epsilon_{\gamma} > \frac{2}{1 - \mu} \frac{1}{\epsilon_s}, \quad (44)$$

of which the minimum value is $1/\epsilon_{\text{max}}$. Photons below this threshold energy $1/\epsilon_{\text{max}}$ never contribute to pair productions, and hence we may put the lower limit of the lowest energy bin, $\beta_0 m_e c^2$, to be $m_e c^2/\epsilon_{\text{max}} = 8.7$ MeV (i.e., $\beta_0 = 1/\epsilon_{\text{max}}$). For the present purpose, it is actually enough to divide the range of ϵ_{γ} into 13 bins and set $\beta_1 = 1.5/\epsilon_{\text{max}}$, $\beta_2 = 2/\epsilon_{\text{max}}$, $\beta_3 = 2.5/\epsilon_{\text{max}}$, $\beta_4 = 3/\epsilon_{\text{max}}$, $\beta_5 = 4/\epsilon_{\text{max}}$, $\beta_6 = 5/\epsilon_{\text{max}}$, $\beta_7 = 10/\epsilon_{\text{max}}$, $\beta_8 = 20/\epsilon_{\text{max}}$, $\beta_9 = 30/\epsilon_{\text{max}}$, $\beta_{10} = 40/\epsilon_{\text{max}}$, $\beta_{11} = 50/\epsilon_{\text{max}}$, $\beta_{12} = 60/\epsilon_{\text{max}}$, and $\beta_{13} = 70/\epsilon_{\text{max}}$. As we shall check in § 3.2, high-energy γ -rays ($\epsilon_{\gamma} > 10/\epsilon_{\text{max}}$) have little influence on the structure of the gap because of their small number density, so that their energy bins are cut coarsely. Moreover, it is enough to put the upper limit of the highest energy bin, $\beta_{13} m_e c^2$, to be $70/\epsilon_{\text{max}} = 609$ MeV for the same reason.

We shall seek the solutions satisfying the boundary conditions (37)–(43), making use of a shooting method. The calculation starts from $x = 0$ with conditions (37)–(39) and is terminated at the *free* boundary at $x = H$ with conditions (40), (41), and (43). In general, condition (42) is not satisfied. To solve this problem, in this paper, we adjust j_0 so that condition (42) may be satisfied.

In a realistic model of a black hole magnetosphere, the electric current flowing along each field line will be determined by a global requirement rather than by microphysics in a localized thin gap, that is, by connecting the load of an outgoing wind or jet to the black hole unipolar inductor (e.g., Thorne et al. 1986). For mathematical simplicity here, we assume that the central point of the gap is located at the

“null surface” where ρ_{GJ} exactly vanishes and impose the symmetry properties around this central point. That is, instead of solving the position of the “inner boundary” ($x = -H$ for a symmetric case), we treat j_0 as a sort of an eigenvalue in a boundary value problem and determine j_0 together with the “outer boundary” position $x = +H$. The analysis made in this paper under the symmetry is, nevertheless, of significance in the sense that we demonstrate explicitly and quantitatively the presence of a stationary pair production cascade in a black hole magnetosphere. Moreover, it will later turn out that the values of j_0 adjusted in the way described above are consistent with what are required for effective energy extraction from rotating supermassive black holes.

The actual scheme is as follows: For very small values of j_0 , for which $|n^+ - n^-|$ is also very small, equation (7) can be approximated as

$$\frac{dE_{\parallel}}{dx} \approx -4\pi A x. \quad (45)$$

Integrating this, we obtain

$$E_{\parallel} \approx E_{\parallel}(0) - 2\pi A x^2. \quad (46)$$

This quadratic solution cannot fulfill condition (42). As j_0 increases significantly, the first term on the right-hand side of equation (7) also increases monotonically with x . Therefore, the shape of $E_{\parallel}(x)$ deviates significantly from equation (46), producing a “brim,” as indicated by the dashed line in Figure 2, in which we choose $U_b = 10^6$ ergs cm^{-3} and $\alpha = 2.0$. As j_0 increases further, dE_{\parallel}/dx at $x = H$ decreases and vanishes at a certain value $j_{\text{cr}}(U_b, \alpha)$. For example, when $U_b = 10^6$ ergs cm^{-3} and $\alpha = 2.0$, j_{cr} becomes 7.4145×10^{-15} abamp cm^{-2} . The solution $E_{\parallel}(x)$ in this case is depicted by the solid line in Figure 2. Above the critical current density j_{cr} , condition (42) could not be satisfied, no matter what initial values of $\Gamma(0)$, $n^-(0)$, and $f_i^-(0)$ ($i = 1, 2, \dots, 13$) we choose. This situation is shown by the dotted line in Figure 2.

To sum up, we shall seek the solutions satisfying equation (42) by adjusting j_0 to $j_{\text{cr}}(U_b, \alpha)$. The resulting system is, then, formed by 29 differential equations (eqs. [7], [8], [18], and [31]) for 31 unknowns (E_{\parallel} , Γ , n^+ , f_1^{\pm} , f_2^{\pm} , \dots , f_{13}^{\pm} , H , and j_0). These should be integrated under 31 boundary conditions (eqs. [37]–[43]).

3. STRUCTURE OF THE POTENTIAL GAP

In the preceding section, we formulated the basic equations and described the procedure to solve them under suitable boundary conditions. Adopting plausible values of external parameters α and U_b , we are now able to solve these equations and investigate the structure of the gap. To begin with, we present typical results of numerical solutions and demonstrate how the current density $j_0 = j_{\text{cr}}$, which sets the rate of the energy extraction from the hole and ensures condition (37), varies with α and U_b in § 3.1. Then we describe somewhat detailed structure of the gap in § 3.2.

3.1. Critical Current Density

To grasp the rough feature, we first show some examples of the solutions of $E_{\parallel}(x)$ in Figure 3. For a fixed value of $U_b = 10^6$ ergs cm^{-3} , we depicted the three cases of $\alpha = 1.5$, 2.0, and 2.5 denoted by the dashed, solid, and dotted lines, respectively. This figure indicates that E_{\parallel} reaches a

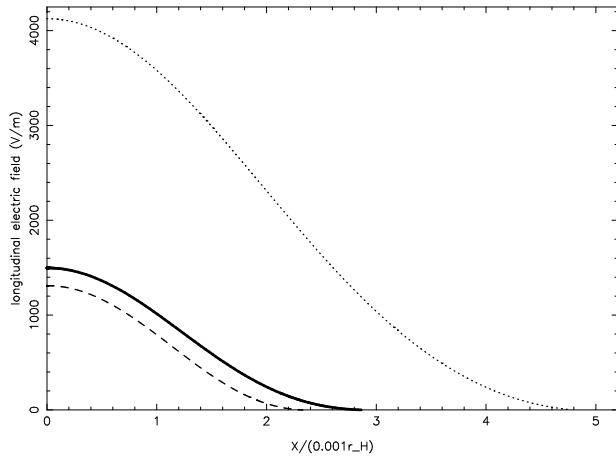


FIG. 3.—Examples of longitudinal electric field $E_{\parallel}(x)$. The abscissa is normalized by $10^{-3}r_H$. The solid line represents the solution corresponding to $\alpha = 2.0$ and is identical with the solid line in Fig. 3. The dashed and dotted lines to $\alpha = 1.5$ and 2.5 , respectively. The energy density of the background radiation field is fixed to be $U_b = 10^6$ ergs cm^{-3} .

maximum at the symmetry point, $x = 0$, decreases monotonically with increasing x , and finally vanishes at the boundary, $x = H$. As we have discussed in § 2.4, the solution $E_{\parallel}(x)$ has a “brim” that makes its derivative at the outer boundary vanish.

Next, let us consider the Lorentz factor $\Gamma(x)$. The result is presented in Figure 4; the parameters are the same as we have chosen in Figure 3. As Figure 4 indicates, the typical values of Γ become several hundreds. This result can be easily understood if we notice that $\Gamma(x)$ is related to $E_{\parallel}(x)$ by equation (8). In most of the gap, except for the vicinity of the boundaries, the right-hand side of equation (8) vanishes in the leading order to give $\Gamma = (eE_{\parallel}/\sigma_T U_b)^{1/2}$. Actually, very close to the boundaries, the monoenergetic approximation is no longer appropriate [i.e., $\Gamma \neq (eE_{\parallel}/\sigma_T U_b)^{1/2}$]; therefore, we must solve the energy dependence of the distribution functions of e^{\pm} s. However, such detailed argument of the e^{\pm} distribution at the boundaries will not be essential for the whole structure of the gap, because the outflowing e^{\pm} s at the boundaries cannot produce γ -rays that can lead to pair production in the gap.

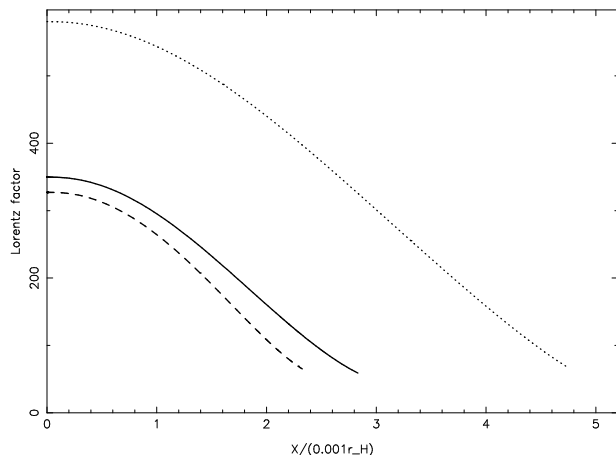


FIG. 4.—Examples of Lorentz factor $\Gamma(x)$. The solid, dashed, and dotted lines correspond to the same parameters chosen in Fig. 3.

As Figures 3 and 4 indicate, the typical half-width of the potential gap is $H \sim 0.005r_H$ for the background radiation field of $U_b = 10^6$ ergs cm^{-3} . However, H has a strong dependence on U_b . This is because the pair production mean free path l_p , which essentially describes H together with the number of γ -rays (N_γ) produced by a single e^+ or e^- via inverse Compton scatterings, strongly depends on U_b . That is, the chance of a γ -ray photon to collide with background soft photons is proportional to U_b ; as a result, l_p increases with decreasing U_b .

The results of H versus α and U_b are summarized in Figure 5, which is one of the main results of this paper. The solid line indicates H versus α for $U_b = 10^6$ ergs cm^{-3} , while the dashed one is for $U_b = 10^5$ ergs cm^{-3} . This figure indicates that H decreases with α for small α (i.e., hard spectrum), but it increases for large α (i.e., soft spectrum). The key point in understanding this behavior is that H is described by l_p/N_γ , pair production mean free path divided by the number of γ -rays produced by a single e^+ or e^- .

Let us evaluate l_p and N_γ at $x = H$. As $f_i^+(x)$ and $\eta_{i,i}$ have already been solved, we can compute l_p from

$$\frac{1}{l_p} = \frac{\sum_{i=1}^{13} \eta_{p,i} f_i^+(H)}{\sum_{i=1}^{13} f_i^+(H)}. \quad (47)$$

For $U_b = 10^6$ ergs cm^{-3} , $\log_{10} l_p/r_H$ versus α at $x = 0$ is depicted by the dash-dotted line in Figure 6. As expected, l_p increases monotonically with α , because the number density of target X -ray photons decrease when the spectrum becomes soft.

The variation of $\log_{10} N_\gamma^{-1}$ is expressed by the dotted line in Figure 6, where N_γ is calculated from

$$N_\gamma = \frac{e}{j_0} \sum_{i=1}^{13} f_i^+(H); \quad (48)$$

N_γ increases (N_γ^{-1} decreases) with α , because the seed UV photons increases as the spectrum becomes soft.

Having observed the variations of l_p and N_γ , we can then go on to consider l_p/N_γ . Figure 6 tells us that $\log_{10} (l_p/r_H)/N_\gamma$, which is plotted by the dash-dotted line, becomes minimum for $\alpha \sim 2$. Moreover, l_p/N_γ describes very well the width of the gap H , of which logarithmic values are plotted by the solid line.

We have seen in this subsection how H depends smoothly on U_b and α . Once that is understood, we are in a better position to evaluate $j_0 = j_{\text{cr}}(U_b, \alpha)$, the conserved current density that carries energy extracted smoothly from the

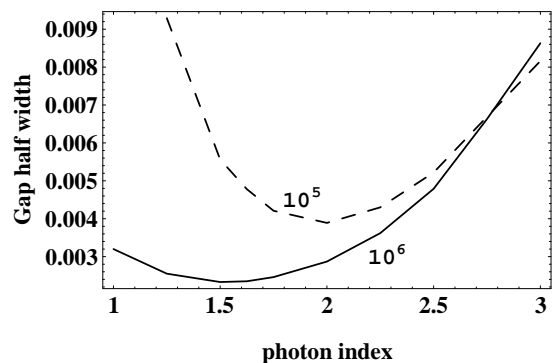


FIG. 5.—Gap half-width H vs. photon index α . The ordinate is normalized by the hole's radius, $r_H = 3 \times 10^{13}$ cm. The solid line describes $H(\alpha)$ for $U_b = 10^6$ ergs cm^{-3} and the dashed line $U_b = 10^5$ ergs cm^{-3} .

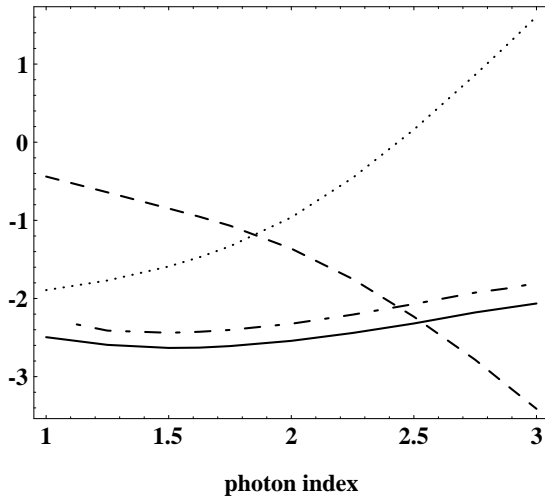


FIG. 6.—The curve of $l_p(\alpha)/r_H$ at $x = 0$ for $U_b = 10^6$ ergs cm^{-3} . The solid line represents $\log_{10}(H/r_H)$, and the dashed, dotted, and dash-dotted lines represent $\log_{10} N_\gamma^{-1}$, $\log_{10} l_p/r_H$, and $\log_{10}(l_p/r_H)/N_\gamma$, respectively.

hole. Equation (42) gives

$$j_{\text{cr}}(U_b, \alpha) = AH; \tag{49}$$

this approximation is valid, because $\Gamma(H) \gg 1$ holds in the gap. Therefore, $j_0 = j_{\text{cr}}(U_b, \alpha)$ can be easily depicted as Figure 7. This figure reveals the fact that *the pair production cascade provides sufficient current density for the effective energy and angular momentum extraction from a rotating supermassive black hole, especially when the background spectrum is soft*. Moreover, j_{cr} , which sets the rate of extractable energy due to the Blandford-Znajek process, becomes large for a less luminous radiation field.

3.2. Detailed Structure of the Gap

Let us now look deeper into other properties of the solutions. First, examples of current densities $en^\pm(x)(1 - 1/\Gamma^2)^{1/2}$ are presented in Figure 8; the parameters are the same ones we chose in Figures 3 and 4. The currents density carried by positrons (or electrons) are depicted by the thick (or thin) lines. The current density difference $e(n^+ - n^-) \times (1 - 1/\Gamma^2)^{1/2}$ increases monotonically with x and reaches its maximum value j_0 at $x = H$, because $n^-(H) = 0$.

Second, an example of $F^\pm(x, \epsilon_\gamma)$ is shown in Figure 9 for $U_b = 10^6$ ergs cm^{-3} and $\alpha = 2$. To avoid complexity, the

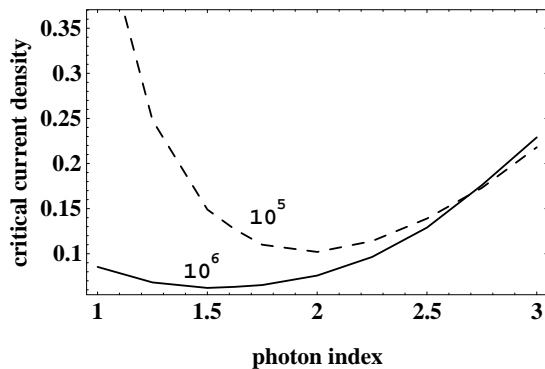


FIG. 7.—Critical current density vs. α . The solid line indicates $j_{\text{cr}}(\alpha)$ for $U_b = 10^6$ ergs cm^{-3} and dashed line for $U_b = 10^5$ ergs cm^{-3} . The ordinate is normalized by 10^{-13} abamp cm^{-2} (cf. eq. [17]).

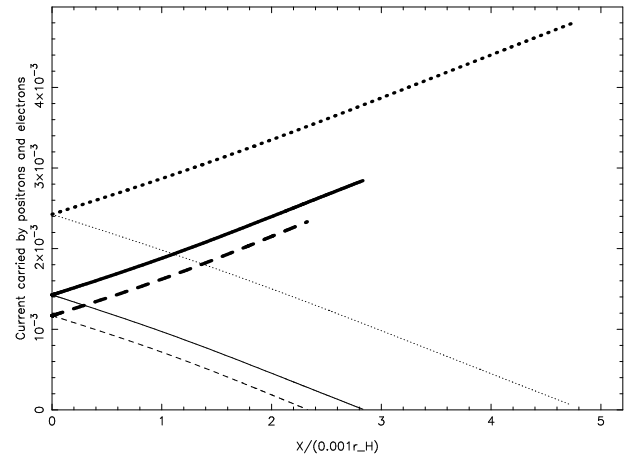


FIG. 8.—Examples of current densities carried by positrons (*thick lines*) and by electrons (*thin lines*) as a function of x . The abscissa is normalized by $10^{-3}r_H$ and the ordinate by 10^{-13} abamp cm^{-2} . The solid, dashed, and dotted lines correspond to the same parameters chosen in Fig. 3.

energy bins are combined into four: the solid line describes γ -ray number density with energies $1/\epsilon_{\text{max}} < \epsilon_\gamma < 2/\epsilon_{\text{max}}$, the dashed one with $2/\epsilon_{\text{max}} < \epsilon_\gamma < 10/\epsilon_{\text{max}}$, the dash-dotted one with $10/\epsilon_{\text{max}} < \epsilon_\gamma < 40/\epsilon_{\text{max}}$, and the dotted one with $40/\epsilon_{\text{max}} < \epsilon_\gamma < 70/\epsilon_{\text{max}}$. We can see from this figure that most of the γ -ray photons are produced in the energy range below $10mc^2/\epsilon_{\text{max}} = 87$ MeV. It must be noted that we could not detect these γ -ray photons because its total luminosity is as small as 10^{24} ergs s^{-1} . The purpose of this paper is to demonstrate that the pair production cascade stationarily supplies a sufficient amount of plasma and enables the energy extraction from a rotating black hole. Therefore, how to produce copious and observable γ -ray photons is not our present concern. They should be produced at more distant regions at several hundred AU (Dermer & Schlickeiser 1993; Schlickeiser & Dermer 1995; BL95; Levinson 1996; Böttcher & Schlickeiser 1996; for ~ 0.4 and less than 0.2 MeV line production, see Skibo, Dermer, & Ramaty 1994)

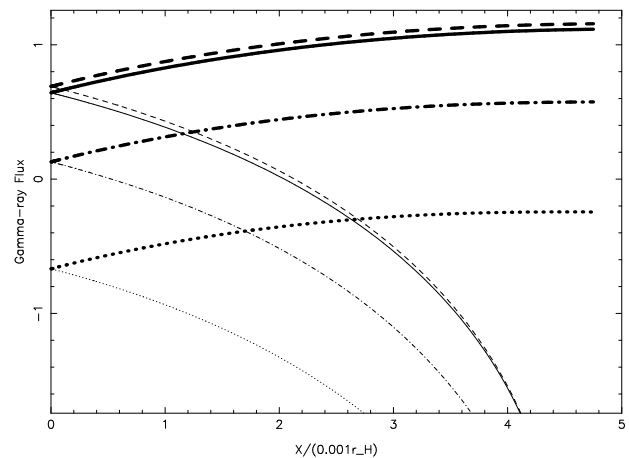


FIG. 9.—An example of $\log_{10} F^\pm(x, \epsilon_\gamma)$. The abscissa is normalized by $10^{-3}r_H$. Thick curves denote the fluxes of γ -rays propagating outward and thin curves those propagating inward. The solid, dashed, dash-dotted, and dotted lines represent the fluxes in the energy range $1/\epsilon_{\text{max}} < \epsilon_\gamma < 2/\epsilon_{\text{max}}$, $2/\epsilon_{\text{max}} < \epsilon_\gamma < 10/\epsilon_{\text{max}}$, $10/\epsilon_{\text{max}} < \epsilon_\gamma < 40/\epsilon_{\text{max}}$, and $40/\epsilon_{\text{max}} < \epsilon_\gamma < 70/\epsilon_{\text{max}}$, respectively. Parameters are chosen to be $\alpha = 2.0$ and $U_b = 10^6$ ergs cm^{-3} .

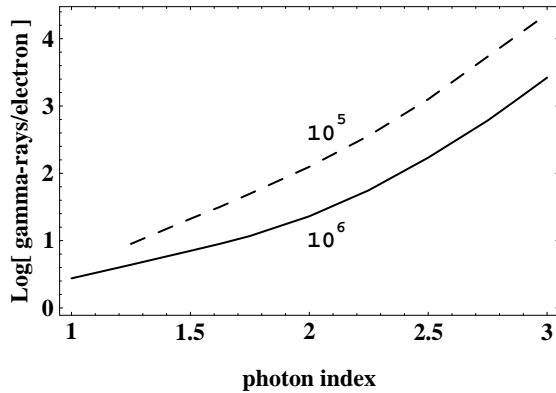


FIG. 10.—Number of γ -rays produced by a single e^+ or e^- , N_γ as a function of α . The solid line denotes $N_\gamma(\alpha)$ for $U_b = 10^6$ ergs cm^{-3} and the dashed line for $U_b = 10^5$ ergs cm^{-3} .

Finally, we shall investigate the number of γ -ray photons produced by a single electron or positron, N_γ . Evaluating N_γ in equation (48), we summarize N_γ versus α and U_b in Figure 10; the parameters are the same ones as we choose in Figure 5. This figure shows the fact that one electron or positron produces typically 10^2 – 10^3 γ -ray photons, that can materialize as pairs. To put it more precisely, N_γ increases with increasing α , because the “seed” photons increases when the spectrum is soft. It is interesting to note that N_γ increases with decreasing U_b . It looks seemingly controversial; however, a less luminous radiation field increases the drag length l_{drag} , and hence $E_{\parallel}(x)$ and $\Gamma(x)$. As a result, the energetic e^\pm s upscatter more soft photons into the energy range $\epsilon_\gamma > 1/\epsilon_{\text{max}}$, above which γ -ray photons collide background X-ray photons to produce pairs. It is for this reason that N_γ increases with decreasing U_b .

4. SUMMARY AND DISCUSSION

In this paper we quantitatively and self-consistently solved the stationary process of a pair production cascade in a thin gap in a rotating black hole magnetosphere. We summarize our results as follows:

1. Under the force-free approximation, the possible position where the electric field along a magnetic field line, E_{\parallel} , arises near the “null surface” where ρ_{GJ} vanishes.

2. Once E_{\parallel} arises, it accelerates migratory or pair-created e^\pm s into ultrarelativistic energies with Lorentz factors $\Gamma = 10^{2.5}$ – 10^4 .

3. An accelerated e^+ or e^- scatters background UV and X-ray photons to produce 10 – 10^3 γ -ray photons of which energies exceed the threshold of pair production.

4. Typically, one of such γ -ray photons (produced by a single e^+ or e^-) collides a background X-ray photon to produce an e^\pm pair, which leads to a pair production cascade.

5. The cascade supplies sufficient amount of pair plasma necessary in maintaining the electric current in the magnetosphere and thus ensures efficient extraction of the hole’s rotational energy in the form of electromagnetic energy.

6. The half-width of the potential gap ($2H$) in which the cascade proceeds is much less than the hole’s radius, r_H . Therefore, the expansion of ρ_{GJ} at $x = 0$ in equation (7) is self-consistently justified.

It will be necessary to make clear the differences between this work and the previous work of Beskin et al. (1992).

They implicitly assumed that all of the γ -ray photons created by the inverse Compton scatterings contribute to the cascade, and they explicitly put $l_p \sim l_c \sim H$. However, as seen in § 3, l_p is much larger than l_c and H . This means that very small fractions of γ -ray photons are enough to maintain the cascade, and most of them escape freely from the gap. This situation is similar to the pair production cascade that is expected to occur in pulsar magnetospheres (e.g., Daugherty & Harding 1982), but it might be dissimilar in that the γ -ray photons from the gap will be unobservable, because, as should be so, the γ -ray flux going out of the gap is negligibly small compared with the outgoing Poynting flux from the hole. Owing to such a difference, Figure 5 differs qualitatively from Figure 6 in Beskin et al. (1992).

In addition to the above difference, we explicitly solved the γ -ray distribution functions by considering their spectrum as shown in Figure 9, whereas in Beskin et al. (1992) the treatment is not explicitly mentioned. It is in fact important to take the γ -ray spectrum into account, because l_p , which essentially controls the gap width together with N_γ , depends strongly on γ -ray energies. However, these γ -rays could not be observed as we have mentioned.

Let us briefly discuss the consistency that the existence of the plasma source gap should not significantly affect the global magnetospheric structure. For one thing, as we have seen, Figure 5 indicates that the half-width of the gap (H) is much smaller than the global length scales, such as r_H . What is more, as Figure 11 indicates, the electric potential drop in the gap is sufficiently small compared with the total electromotive force (EMF), $\sim 10^{19} \text{V} (a/M)(M/10^8 M_\odot)(B/10^4 \text{G})$. Even for the less luminous case of $U_b = 10^5$ ergs cm^{-3} , in which current density j_0 allows the most effective energy extraction from a rotating supermassive black hole, the potential drop in the gap is as small as 0.1% of the total EMF.

It will be of interest to contrast the cascade processes of producing γ -rays and e^\pm plasma presumed to operate in the two different locations. The first one is necessary to maintain the Poynting flux throughout the force-free domain, by working in the much localized thin gap deep inside the magnetosphere just above the horizon. The plasma in the gap is more or less charge-separated, and the charge density is less than ρ_{GJ} . On the other hand, the second works on a much more large scale, much above the horizon, to convert the Poynting flux to the kinetic energy of bulk motion of the jet above which is superposed the relativistic motion of e^\pm

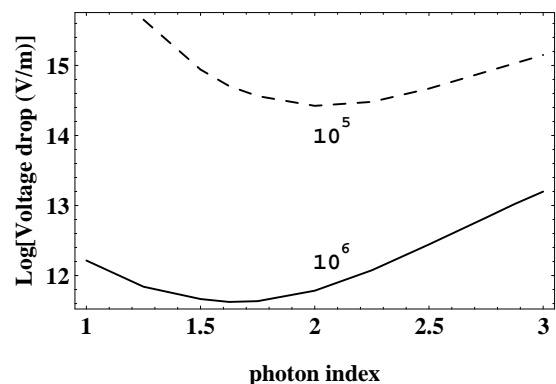


FIG. 11.—Total voltage drop in the gap as a function of α . The solid line corresponds to the case of $U_b = 10^6$ ergs cm^{-3} and the dashed line to that of $U_b = 10^5$ ergs cm^{-3} .

plasma and γ -rays. The collimation process must simultaneously be incorporated, e.g., because of the pinching effect of magnetic field and/or due to external confining force of the wind from the disk.

In this paper, we have assumed that all the e^\pm s at x move with the same Lorentz factor $\Gamma(x)$. However, it may be debatable whether we can neglect the existence of nonrelativistic e^\pm s. That is, freshly produced e^+ s (or e^- s) having momenta in the opposite (same) direction of E_\parallel are decelerated to turn back in very short lengths. Such nonrelativistic e^\pm s that turn back may not be negligible in the Maxwell equation (7) because of their small velocity. For example, at $x > 0$, freshly produced e^\pm s have preferentially positive momenta, because the γ -ray flux in the $+x$ -direction exceeds that in the $-x$ -direction. As a result, nonrelativistic e^- s, which are turning back, may dominate nonrelativistic e^+ s to enhance the screening of E_\parallel . This is because the density of the nonrelativistic e^- s appears as a negative term in the Maxwell equation to contribute in the same sense as $-Ax$ term at $x > 0$. Such an effect is actually negligible in the central region of the gap where E_\parallel is large, because the nonrelativistic e^\pm s turn back so quickly that their density could not overcome that of relativistic e^\pm s. However, the existence of nonrelativistic e^\pm s may become significant close to the boundaries ($x \approx \pm H$), because the small electric field E_\parallel there increases the length of turning back and hence the density of nonrelativistic particles. Therefore, taking account of nonrelativistic e^\pm s may alter the boundary structure and reduce the gap width to some extent. However, the

essential features of pair production cascade will not be lost in disregard of nonrelativistic e^\pm s, because the cascade is mainly governed by the gap structure where E_\parallel is sufficiently large. Nonrelativistic e^\pm s may induce space-charge-density waves outside the boundary (Shibata 1997) and may become important when we consider the problem how to embed the potential gap in a Goldreich-Julian flow.

It might finally be interesting to investigate whether or not the same mechanism works around a stellar-mass black hole, from which the rotational energy may be extracted, resulting in a galactic γ -ray jet (cf. Levinson & Blandford 1996). Around a supermassive black hole, which is the concern of this paper, the relaxation length, l_{drag} , at which e^\pm s lose their perpendicular momenta owing to scatterings with background UV photons is much smaller than l_p , l_c , and H . Therefore, particle motion and γ -ray behavior can be treated one-dimensionally; in addition, electron/positron spectra are approximated by monoenergetic ones. However, as Beskin et al. (1992) pointed out, around a stellar-mass black hole, neither the drag due to background photons nor the synchrotron loss cannot make the motion of e^\pm s be one-dimensional, because their mean free paths are much larger than l_c or H . This issue will be our next target.

One of the authors (K. H.) wishes to thank Drs. S. Shibata and M. Takahasi for valuable comments and criticisms. The authors thank the Astronomical Data Analysis Center of National Astronomical Observatory, Japan, for the use of workstations.

REFERENCES

- Beskin, V. S., Istomin, Ya. N., & Par'ev, V. I. 1992, *Soviet Astron.*, 36(6), 642
 Berestetskii, V. B., Lifshitz, E. M., & Pitaevskii, L. P. 1989, *Quantum Electrodynamics* (3d ed., Japanese trans.; Tokyo: Maruzen)
 Blandford, R. D. 1976, *MNRAS*, 176, 465
 ———. 1989, in *Theory of Accretion Disks*, ed. P. Meyer, W. Duschl, J. Frank, & E. Meyer-Hofmeister (Dordrecht: Kluwer), 35
 ———. 1993, in *AIP Conf. Proc. 280, Proceedings of the Compton Symposium 1992*, ed. M. Friedlander, N. Gehrel, & D. J. Macomb (New York: AIP), 553
 Blandford, R. D., & Levinson, A. 1995, *ApJ*, 441, 79 (BL95)
 Blandford, R. D., & Znajek, R. L. 1977, *MNRAS*, 179, 433
 Böttcher, M., & Schlickeiser, R. 1996, *A&A*, 306, 86
 Daugherty, J. K., & Harding, A. K. 1982, *ApJ*, 252, 337
 Dermer, C. D., & Schlickeiser, R. 1993, *ApJ*, 416, 458
 Levinson, A. 1996, *ApJ*, 467, 546
 Levinson, A., & Blandford, R. D. 1996, *ApJ*, 456, L29.
 Lovelace, R. V. E. 1976, *Nature*, 262, 649
 Macdonald, D. A., & Thorne, K. S. 1982, *MNRAS*, 198, 345
 Okamoto, I. 1992, *MNRAS*, 254, 192
 Rybicki, G. B., & Lightman, A. P. 1979, *Radiative Processes in Astrophysics* (New York: Wiley)
 Schlickeiser, R., & Dermer, C. D. 1995, *A&A*, 300, L29
 Shibata, S. 1997, *MNRAS*, 287, 262
 Skibo, J. G., Dermer, C. D., & Ramaty, R. 1994, *ApJ*, 431, L39
 Thorne, K. S., Price, R. H., & Macdonald, D. A. 1986, *Black Holes: The Membrane Paradigm* (New Haven: Yale Univ. Press)
 von Montigny, C., et al. 1995, *ApJ*, 440, 525